Timewise Temperature Control with Heat Metering using a Thermoelectric Module

M.A. Ahamat, M.J. Tierney

Accepted Manuscript

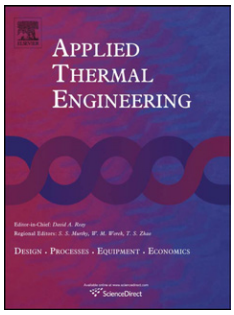

Title: Timewise Temperature Control with Heat Metering using a Thermoelectric Module

Authors: M.A. Ahamat, M.J. Tierney

PII: S1359-4311(11)00011-1

DOI: 10.1016/j.applthermaleng.2011.01.002

Reference: ATE 3366

To appear in: *Applied Thermal Engineering*

Received Date: 29 July 2010

Revised Date: 29 December 2010

Accepted Date: 4 January 2011

Please cite this article as: M.A. Ahamat, M.J. Tierney. Timewise Temperature Control with Heat Metering using a Thermoelectric Module, Applied Thermal Engineering (2011), doi: 10.1016/j.applthermaleng.2011.01.002

Timewise Temperature Control with Heat Metering using a Thermoelectric Module

M A **Ahamat***, M. J. **Tierney**

Department of Mechanical Engineering, Queen's Building, University of Bristol, University Walk, Bristol, BS8 1TR, United Kingdom

Phone: +44 (0)117 331 5903

Fax: +44 (0)117 331 7642

*Email: ma4316@bristol.ac.uk

ABSTRACT

A thermoelectric module was adapted to (1) control the face temperature of an aluminium sample as a function of time, and (2) measure the associated instantaneous rate of heat transfer into the sample. Proportional (P) or Proportional-Integral-Derivative (PID) controls were applied. With respect to time, constant temperature, sinusoidal and triangular temperature variations were tested. These temperatures were well within 0.1 K of the set point (one standard error). Tests on square wave temperature variation indicated the limitations of the module heating and cooling power. For the range of temperatures explored, the thermoelectric properties of the module were found by fitting predicted temperatures to experimental measurements (the module electrical resistance was taken from the manufacturer's data). Associated uncertainty, typically ± 10% of total heat flow at 12 Watt, was far bigger than the ± 2% for heat flow meters assessed against National Institute of Standards and Technology (NIST) calibrations; nonetheless the temporal resolution (3 readings per second) offers some useful insight into thermal processes.

KEYWORDS: thermoelectric module, temperature control, heat transfer.

NOMENCLATURE

Symbol	Description (Unit)
a	Amplitude of the sine wave (K)
A_{al}	Area of aluminium sample for heat transfer (m^2)
A_m	Area of thermoelectric module surface (m^2)
h_f	Thermal transmittance between thermoelectric module and aluminium sample ($kW\ m^{-2}\ K^{-1}$)
I	Current through thermoelectric module (Ampere)
k_{al}	Thermal conductivity of aluminium ($Wm^{-1}K^{-1}$)
$\mathbf{k'}$	Effective thermal conductivity of thermoelectric module ($W\ m^{-1}\ K^{-1}$)
N	Number of junction pairs in the thermoelectric module (-)
$\mathbf{Q_f}$	Instantaneous inferred heat flow across thermoelectric module surface (W)
$Q_{filtered}$	Filtered instantaneous inferred heat flow across thermoelectric module surface (W)
$\mathbf{R_m}$	Electrical resistance of thermoelectric module (ohm)
$\mathbf{R_w}$	Electrical resistance of the wires leading to thermoelectric module (ohm)
t	Time (s)
$\mathbf{T_f}$	Estimated thermoelectric module face temperature (thermodynamic value) (K)
T_o	Centre of amplitude of temperature variation (K)
$T_{controller}$	Temperature feedback into the P/PID controller (K)
TC1	Measured block temperature at position 1 (K)
TC2	Measure block temperature at position 2 (K)
T(t)	Set point temperature (K)
V	Potential difference across thermoelectric module (V)
w	Effective thickness of thermoelectric module (m)
x_{f1}	Distance from TC1 to aluminium block/thermoelectric module interface (m)
Y_n	Predicted aluminium block temperature for node n = 1 to 11 (K)
α	Seebeck coefficient ($V\ K^{-1}$)
Δt	Time interval between two consecutive control signals (s)
θ	Temperature different between thermoelectric module surfaces (K)
ω	Angular velocity of the sine wave ($rad\ s^{-1}$)

1. INTRODUCTION

In measurement, it is sometimes useful to control the face temperature of a sample as a function of time such as $T(t) = T_0 + a \sin(\omega t)$. For example, the thermal diffusivity of a solid can then be inferred from the phase difference between temperature signals at different distances from the face [1, 2]. Alternatively, such a controller would facilitate experiments on

dynamic mass transfer into a sample by producing an oscillating liquid temperature and consequently an oscillating saturation vapour pressure. Thermoelectric modules are attractive for this purpose because the heating direction is reversed electronically and smoothly, avoiding the valve switching associated with fluid heat transfer media. We intend later to use this reported device to assess the rates of heat transfer from adsorbent coated surfaces, similar to those employed in heat-operated adsorption chillers. This would give a direct assessment of thermal performance of the system of surface-binder-sorbent, rather than separate assessments of adsorbent isotherm, and thermal resistance of sorbent and sorbent-to-surface bond. Importantly, one expects measurement to capture the exponential decay of heat transfer rate with respect to time [3].

To date, commercial thermoelectric module temperature controllers have been dedicated to maintaining a temperature set point. Thermoelectric modules control the temperatures of medical cooling kits for blood or vaccine storage at between 6 and 10 ^{o}C, heating the kit to 37 ^{o}C prior to use [4]. The surface temperature of a thermoelectric module is controlled within 0.1 K by means of an average linear dynamic model of the thermoelectric cooler, a pseudo derivative feedback control structure and disturbance rejection [5]. Car seats are maintained at a set temperature, some fluctuations are apparent during the heating mode [6]. Cascading arrangements of thermoelectric module are applied to boxed electrical circuit boards for testing in the range between -40 ^{o}C and +55 ^{o}C, with precision of 0.5 K[7]. In all such systems, careful tuning of the PID controller parameter is strongly advised[8].

Thermoelectric modules are employed as known heat sources to determine the thermal conductivity of low thermal conductivity materials and tropical food [9]. When operated as thermopiles, they offer a relatively high output voltage, detecting heat fluxes at temperatures down to -213.15 ^{o}C [10].

Our principal goal was the implementation of a changing set point. The secondary objective of our work was to test the usefulness of the thermoelectric module for instantaneous heat flux measurement. An apparatus is reported here. In the absence of active control, the cooling curve of the sample could be predicted consistently well and data-fitted to yield thermoelectric properties. The quality of control of several temperature waveforms is presented before rates of heat flow.

2. APPARATUS

The subsystems developed were hardware, electronics and data management, and control algorithms. Figure 1 shows the block diagram of the complete system.

Figure 1

2.1 Hardware

Figure 2 is a schematic arrangement of the apparatus used. The thermoelectric module was manufactured by Melcor (Model: CP1.4-127-06L). The 6082-T6 aluminium alloy sample measured 40 mm x 40 mm x 50 mm and weighed 217 gram. The thermal conductivity of 6082-T6 is 170 $Wm^{-1}K^{-1}$ [11] with specific heat capacity of 900 J $kg^{-1}K^{-1}$ [12]. TC1 and TC2 indicate slots for Type K thermocouples, 5 and 45 mm from the sample-to-module interface. Thermocouple TC1 provided the temperature feedback to the P or PID controller. Electrolube HTCP compound was applied at both faces of the thermoelectric module. The heat sink was rated at 0.13 to 1.6 K W^{-1} and equipped with a 12 Watt fan. The insulation was fabricated from expanded polystyrene, measuring 40mm thick.

Figure 2

2.2 Electronics

Figure 1 shows the control system in block diagram form. In essence, signals from the sample (TC1) were processed and compared against a set point (T (t)) in order that the necessary potential difference across the module might be determined. The power supply was built around a robot electronics MD03 H-bridge applying Pulse Width Modulation at 15 kHz. Strong electrical interference ensued so that all modules were necessarily encased in aluminium boxes; a pair of (hand wound) 1.2 millihenry coils was connected to the MD03 H-bridge. The thermocouple signal was amplified by an AD 595 integrated circuit, intended for Type K thermocouples, and further by an LM741 circuit to give 0.1 V K^{-1} sensitivity. Given high levels of electrical noise, amplifiers were conditioned with 540 millihenry coils reducing noise to 0.02 V (after amplification).

2.3 Data management and control algorithms

Data management comprised a Labjack U12 module, offering four digital I/O screw terminals, eight 12-bit analogue inputs and two 12-bit control analogue outputs. Proportional control was applied when the set point error exceeded 1 K, otherwise PID control was applied, originally tuned using the Ziegler-Nichols method. The temperature feedback into the controller was taken from the average of three consecutive measurements of TC1,

$T_{controller}(t) = [TC1(t) + TC1(t-\Delta t) + TC1(t-2\Delta t)] / 3$ and $\Delta t = 0.333$ second.

Each set of thermocouple-plus-amplifier was calibrated against a PT100 thermometer (accuracy 0.03 K), and the corresponding correction factor was within 0.1 K.

3. ANALYSIS, CALIBRATION AND COOLING CURVE

These closely coupled parts of the work are reported in the same section. The heat transfer at the module face (Q_f) was needed to calibrate the experiment (Section 3.2) and as a useful signal (Section 5).

3.1 Theoretical background

Ioffe [13] gives heat transfer as:

$$Q_f = \alpha N I T_f + 0.5 I^2 R_m - \frac{A_m k' \theta}{w} \quad (1)$$

where positive Q_f indicates heating of the sample and the three groups on the right hand side represent respectively Peltier effect, Ohmic heating, and thermal conduction between module faces. (Here, please note that T_f indicates a thermodynamic temperature, measured in Kelvin). With regard to the independent variables, current (I) was measured whereas the temperature difference between faces followed from Equation 2.

$$\Theta(t) = \frac{V(t) - I(t)(R_m(t) + R_w)}{N\alpha} \quad (2)$$

The face temperature was not measured directly but followed from Equation 3.

$$T_f = TC1 + \frac{Q_f}{A_{al}} \left(\frac{1}{h_f} + \frac{x_{f1}}{k_{al}} \right) \quad (3)$$

The module electrical resistance (R_m in Equation 1) was taken as a linear function of average module temperature ($T_f + \Theta/2$) using manufacturer's data. The transmittance of conductive grease (h_f in Equation 3) had been previously measured as 12.5 kW m^{-2} K^{-1}, using the ASTM D5470 method. (The grease sample was bounded by aluminium surfaces.)

3.2 Procedure and data analysis

In calibrations, the sample was bonded to the face of the thermoelectric module, insulated thermally and controlled at 50 ^{o}C for 30 minutes before cooling to -7 to -14 ^{o}C by means of a constant potential difference applied across the module (Figure 3).

To establish αN and $A_m k'/ w$, the procedure was:

1) Tentatively estimate αN
2) For steady state (2500 s ≤ t ≤ 3000 s in Figure 3(a)), estimate heat losses across insulation and attribute to Q_f
3) For steady state (2500 s ≤ t ≤ 3000 s in Figure 3(a)) obtain T_f from Equation 3, Θ(t) from Equation 2 and $A_m k'/ w$ from Equation 1 (manipulated)
4) For all times (0 s ≤ t ≤ 3000 s in Figure 3(a)), predict sample internal temperatures numerically using estimated face heat flow Q_f (I, V, T_f) from Equation 1 as a boundary condition. (An explicit finite difference method with 11 nodes yielded temperature predictions, Y_n, where n is node serial number).
5) For the two measurement locations and all measurement times, find the root mean square error (RMS) of TC1 – Y_2 and TC2 – Y_{10}.
6) Repeat the procedure for a range of trial values of αN, establishing a point of minimum RMS error.

Figure 3(a) shows a cooling curve, comparing measured and predicted temperatures TC1 and Y_2. (The optimised values of αN and $A_m κ'/w$ listed on Figure 3 pertain to this particular experiment). For a set of six calibrations αN = 0.0543 ± 0.00059 V K^{-1} and $A_m κ'/w$ = 10.08 ± 0.13 W K^{-1} (confidence intervals correspond to one standard deviation). These standard deviations were employed with other measurement uncertainties (Table 1) in

a Monte Carlo simulation of the calibration experiment. The inferred heat flow had 10% uncertainty (for Q_f = 12 W). This contrasts with estimates of 2% error for proprietary heat flux meters as measured at NIST using steady radiative heat flow [14] or 3% considering unsteady spray cooling [15].

Figure 3

Table 1

4. TEMPERATURE CONTROL

This section considers the capability of equipment to maintain constant, square, sine and triangular waveforms of temperature against time. In all experiments, the laboratory air (19 ^{o}C to 27 ^{o}C) acted as the thermal reservoir. For most experiments the applied current was less than 1.5 Ampere versus the manufacturer's maximum rating (6 Ampere yielding maximum cooling power of 51.4 Watt). The attempts to follow a square wave set point formed an exception with maximum current of 3 Ampere at the temperature rise or fall.

4.1 Control to a constant temperature

The sample temperature was controlled at a fixed set point as in Table 2 for 6670 seconds. The worst deviation from set point was 0.176 K (3 standard errors) versus measurement noise of 0.114 K on the same basis. This compares favourably with the deviation of 0.1 K reported elsewhere[16].

Table 2

4.2 Controls to achieve time varying temperature

The square wave is a severe test since in principle an instantaneous temperature change demands an infinite flow of heat. Hence temperature undershoots were inevitable (Figure 4). On settling, the sample temperature was within 0.2 K of set point.

Figure 4

The sinusoidal and triangular temperature variation against time were tested for 10 cycles with amplitude of 7 K, centre of amplitude of 30 ^{o}C and period of 667 seconds. For the

sinusoidal temperature variation (Figure 5), the integral parameter was doubled from the Ziegler Nichols value to minimise an oscillating error at heating and cooling phase. Thereafter the sample temperature was within 0.176 K of its set point (3 standard errors). For the triangular waveform (Figure 6), the abrupt temperature change promoted temporary overshoots at the vertex but these did not exceed 0.55 K, and on average the sample temperature was within 0.27 K of its set point (3 standard errors).

Figure 5

Figure 6

5. EVALUATION OF TIME VARYING HEAT FLOW

For the sinusoidal pattern in Figure 5, the corresponding heat pumping was deduced from Equation 1 (see Figure 7). The inferred heat transfer was highly susceptible to (small) thermocouple signal noise. Thus Q_f was filtered by $Q_{filtered}(t) = 0.1\ Q_f(t) + 0.9\ Q_{filtered}(t-\Delta t)$ with time constant of 3.33 seconds, reducing the RMS error from 2.13 Watt (Figure 7) to 1.28 Watt(Figure 8). The ratio of RMS error divided by the magnitude of inferred heat before and after filtering was 16.5% and 10.0% respectively, comparable with our previous error analysis.

Figure 7

Figure 8

The accuracy of inferred instantaneous heat flow is poorer than the typical accuracies for heat flow meters. However, coupling active temperature control and heat measurement obviates the requirement for additional heat flux meters, and omitting the heat capacity of the meter will provide better transmittance between thermoelectric module and the controlled body.

Our proposed method is therefore useful for transient heat transfer problems, such as heat rejection from sorbent materials, where response time is as important as heat transfer. In future papers we intend to report on the incorporation of a heat-flux-meter into the equipment and its impact on control.

6. CONCLUSIONS

Sample temperatures were controlled as constant or changing as a function of time. Standard errors from set point were less than 0.06 K for constant condition and sinusoidal variation, and less than 0.1 K for the triangular temperature variation. The latter suffered slightly from overshoots at the vertexes (Figure 6). The sample temperature (expectedly) failed to follow a square wave owing to limited power. For sample cooling under constant applied potential difference (V), inferred estimates of αN and $A_m k'/w$ were repeatable to ~1%. Thereupon, according to our error analysis (by Monte Carlo) the compounded effect of all uncertainties on heat transfer was 10.0%. For controlled, cyclic temperatures the signal noise perturbed control such that the uncertainty became 16.5%, reducing to the previously mentioned 10.0% with filtering (time constant = 3.33 s only).

Acknowledgements

The authors acknowledge financial support from the Malaysian Government, Majlis Amanah Rakyat (MARA) and Universiti Kuala Lumpur. The hard work and electronic designs of Mr Mark Fitzgerald and the assistance of Mr Clive Wishart are gratefully acknowledged.

REFERENCES

1. Angstrom, A.J., New method of determining the thermal conductibility of bodies. Philosophical Magazine, 1863. **25**(4): 130-142.
2. King, R.W., A method of measuring heat conductivities. Physical Review, 1915. **6**: 437-445.
3. Ahamat, M.A. and M.J. Tierney, Development of the Calorimetry Method in Assessing the Performance of Coated Fin in Innovative Materials for Processes in Energy Systems 2010. Research Publishing: Singapore.74-78.
4. Guler, N.F. and R. Ahiska, Design and Testing of A Microprocessor-controlled Portable Thermoelectric Medical Cooling Kit. Applied Thermal Engineering, 2002. **22**: 1271-1276
5. Huang, B.J. and C.L. Duang, System dynamic model and temperature control of a thermoelectric cooler. International Journal of Refrigeration, 1999. **23**: 197-207.
6. Choi, H.-S., S. Yun, and K.-i. Whang, Development of a temperature-controlled car-seat system utilizing thermoelectric device. Applied Thermal Engineering, 2006. **27**: 2841-2849.
7. Qi, Y., Z. Li, and J. Zhang, Peltier temperature controlled box for test circuit board in 22nd International Conference on Thermoelectrics. 2003, IEEE Xplore: La Grande Motte, France. 644-647.
8. Optimizing thermoelectric temperature control systems. 1995, Wavelength Electronics Inc.
9. Gonzalez-Mendizabal, D., P. Bortot, and A.L.L.d. Ramos, A Thermal Conductivity Experimental Method Based on the Peltier Effect. International Journal of Thermophysics, 1998. **19**: 1229-1238.
10. Haruyama, T., Performance of Peltier elements as a cryogenic heat flux sensor at temperature down to 60 K. Cryogenics, 2001. **41**: 335-339.
11. Aluminium 6082-T6, MatWeb, The Online Material Database, 2010.
12. Kessler, O. and M. Reich, Similarities and Differences in Heat Treatment Simulation on Aluminium Alloys and Steels. Mat.-wiss. u. Werkstofftech, 2009. **40**: 473-478.
13. Ioffe, A.F., Semiconductor Thermoelements and Thermoelectric Cooling. 1957: Infosearch Limited London.
14. Murthy, A.V., B.K. Tsai, and R.D. Saunders, Radiative Calibration of Heat-Flux Sensors at NIST: Facilities and Techniques. Journal of Research of the National Institute of Standards and Technology, 2000. **105**: 293-205.
15. Sabau, A.S. and Z. Wu, Evaluation of a heat flux sensor for spray cooling for the die casting processes. Journal of Materials Processing Technology, 2007. **182**: 312-318.
16. Riffat, S.B. and X. Ma, Thermoelectrics:A review of present and potential applications. Applied Thermal Engineering, 2003. **23**: 913-935.

Table 1: Uncertainties in error analysis

Term	Mean value	Steady error	Non-steady error	Comments
	0.0543 V K^{-1}	1.08 %	-	One standard deviation
$\frac{\alpha N}{A_m k'}{}_w$	10.08 W K^{-1}	1.29 %	-	from 6 experiments
I	-	0.65 %	0.65 %	Manufacturer data sheet
T_f	-	0.05 K	0.1 K	Experiment
V	-	0.005 V	0.005 V	Experiment
R	-	-	-	Related to I, T_f and V

Table 2. Set point and standard error of temperature controls at constant temperature

Run Number	Set point(^{o}C)	Standard Error(K)
1	2.0	0.0530
2	2.0	0.0444
3	38.0	0.0587
4	38.5	0.0470

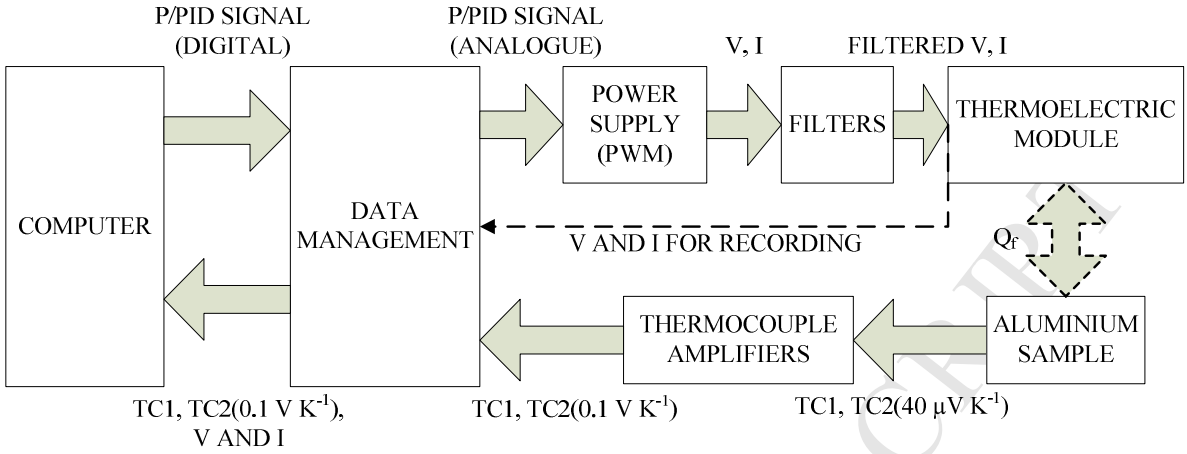

Figure 1. Block diagram of system

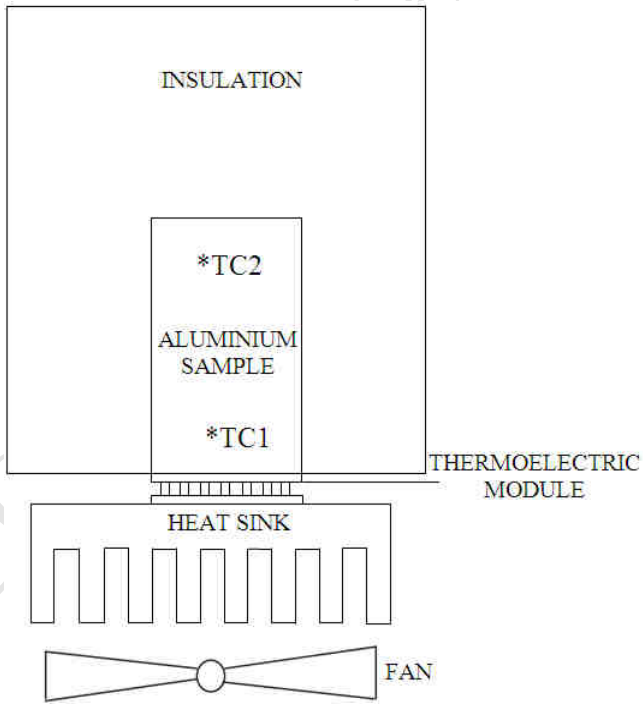

Figure 2. Schematic of experimental arrangement

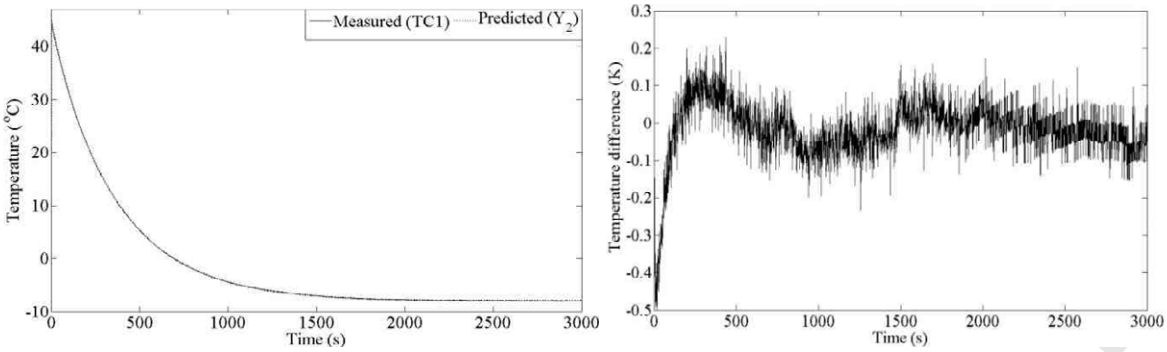

(a) (b)

Figure 3. Typical cooling curve and corresponding temperature prediction (V=4.57 volt, $\alpha N = 0.05425$ V K^{-1}, $A_m k'/ w = 9.99$ W K^{-1}) (b) difference between measured and predicted temperature ($TC1 - Y_2$)

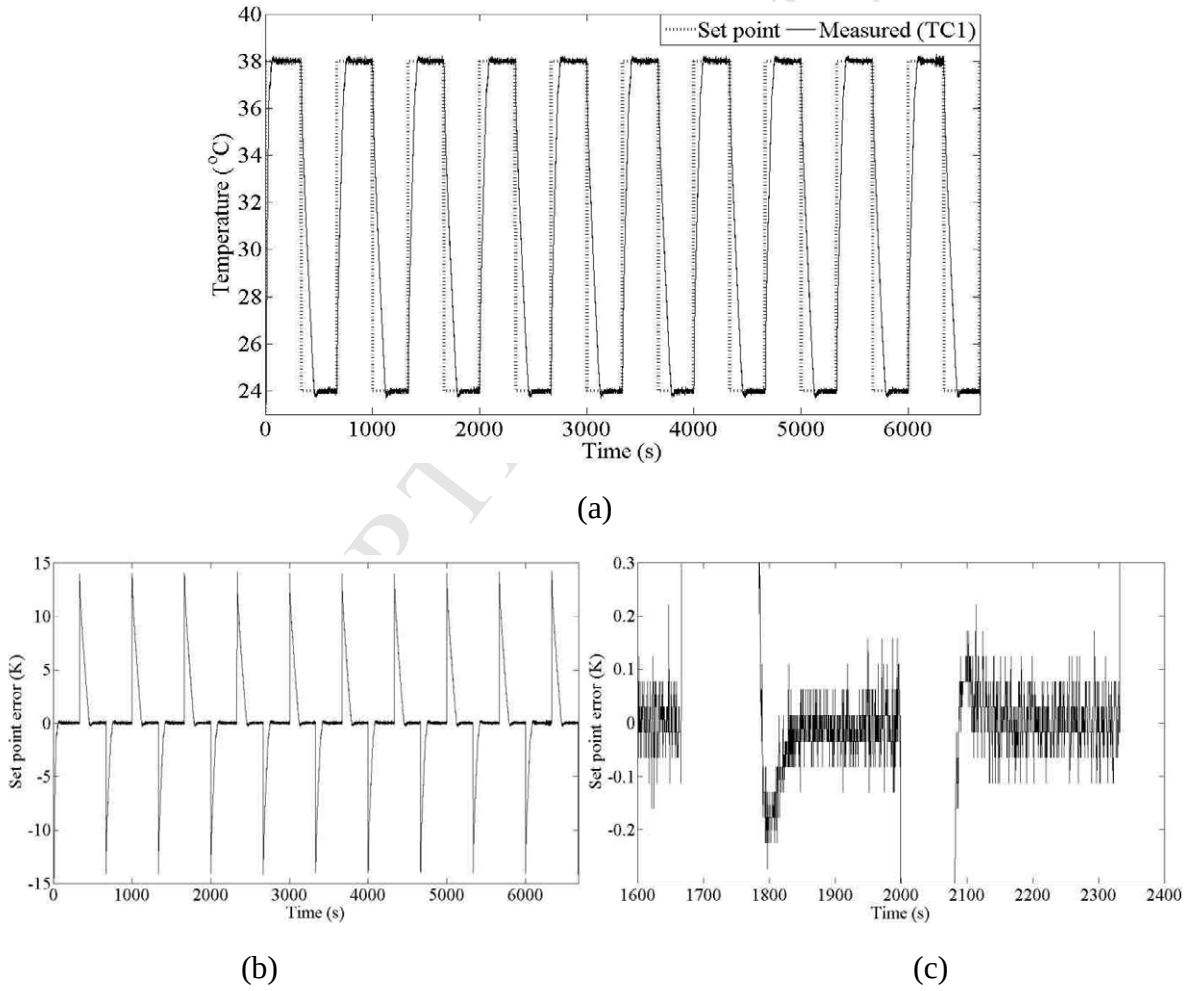

(a)

(b) (c)

Figure 4. Response to square-wave set point (a) sample and set point temperature (b) set point error (c) enlarged view of set point error

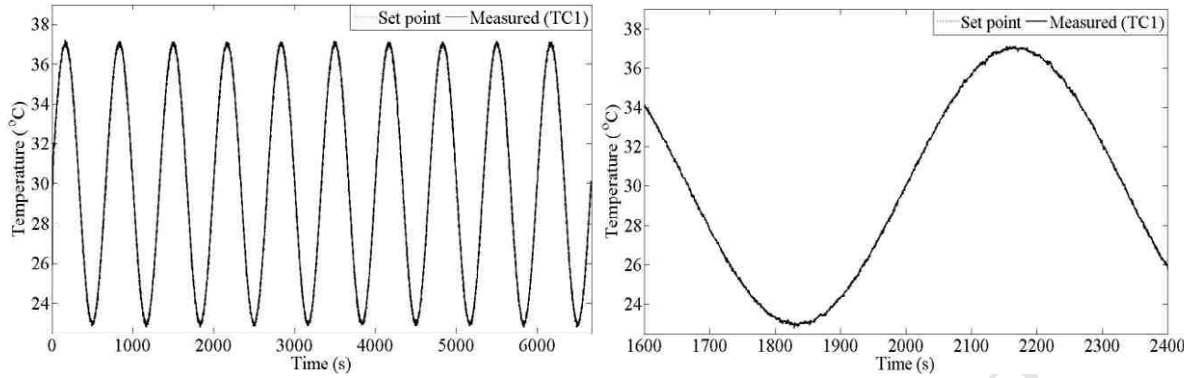

(a) (b)

Figure 5. Response to a sinusoidal set point (a) full experiment (b) enlarged view

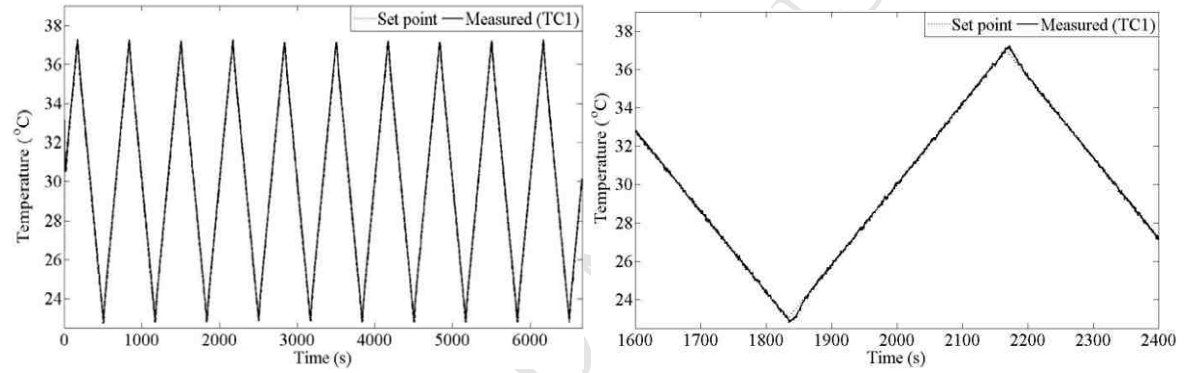

(a) (b)

Figure 6. Response to triangular set point (a) full experiment (b) enlarged view

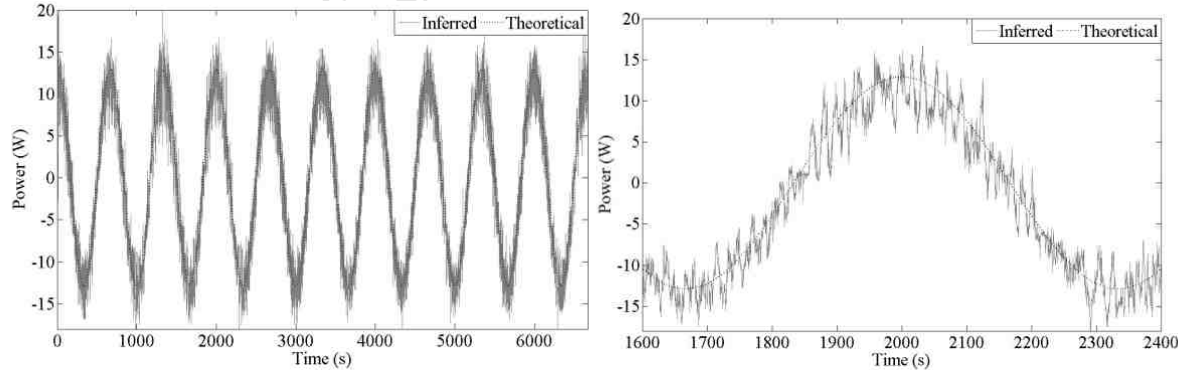

(a) (b)

Figure 7. Heat transfer inferred for sinusoidal set point (a) full experiment (b) enlarged view

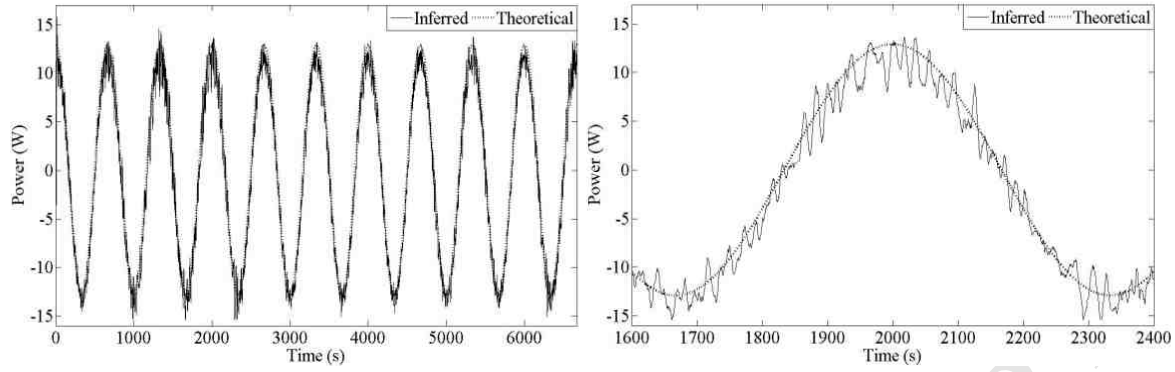

(a) (b)

Figure 8. Data from Figure 7 with filter (time constant = 3.33 s) (a) full experiment (b) enlarged view